POAC'25
St. John's, Newfoundland and Labrador, Canada

Proceedings of the 28th International Conference on Port and Ocean Engineering under Arctic Conditions
Jul 13-17, 2025
St. John's, Newfoundland and Labrador
Canada

Numerical Analysis of Dynamic Ice Submersion Force Acting on Heavy Icebreaker

Wenbo Dong[1], Fang Li[1], Shifeng Ding[2], Pentti Kujala[1,3], Guangwei He[4], Shixiao FU[1], Li Zhou[1,*]

[1] State Key Laboratory of Ocean Engineering, Shanghai Jiao Tong University, Shanghai, China

[2] School of Naval Architecture, Ocean & Civil Engineering, Shanghai Jiao Tong University, Shanghai, China

[3] Estonian Maritime Academy, Tallinn University of Technology, Tallinn, Estonia

[4] Guangzhou Shipbuilding International Co., Ltd., Guangzhou, China

ABSTRACT

Submerged resistance constitutes a significant portion of ice resistance. Accurate and rapid simulation of ice motion trajectories under ship-ice interaction and prediction of submerged resistance are crucial for ensuring ship navigation safety and optimizing icebreaker hull designs. Traditional empirical formulas for resistance prediction may not be suitable for scenarios involving heavy icebreakers operating in conditions of thicker ice and higher speeds. This study develops a simulation model for ship towing in pre-sawn ice based on the non-smooth discrete element method. Efficient collision detection and iterative solving of the Mixed Linear Complementarity Problem are employed to calculate collision impulses between ship-ice and ice-ice interactions. Real-time buoyancy calculation is introduced, and a parameter-free model for ice lift and drag forces is established based on the Morison equation and experimental data, enabling accurate computation of hydrostatic and hydrodynamic forces acting on the ice. Simulations of a heavy icebreaker towed in pre-sawn ice under varying ice thicknesses and ship speeds were conducted. The results demonstrate that the model can well predict the motion trajectories and distribution of ice under ship-ice interaction. At low speeds, ice accumulates at the bow and reunites at the stern. At high speeds, some ice is pushed away at the bow, preventing further contact with the hull, while ice separation occurs at the stern. At low ice thickness, the simulated submerged resistance trend matches well with empirical formulas. However, at high ice thickness, ice resistance is about 20% higher than the Lindqvist formula's results. Traditional empirical formulas need further improvement, and this method requires more experimental validation. The proposed model can predict submerged resistance and provides an efficient tool for hull line optimization.

KEY WORDS Heavy icebreaker; Pre-sawn ice; Ice force; Submersion; NDEM.

INTRODUCTION

The ship-ice interaction is a complex dynamic process. Valanto (1989) has categorized the ice-breaking process into four sequential phases based on the temporal order of ship-ice interaction: the crushing phase, the bending failure phase, the rotation and submersion phase, and the sliding phase. The first three phases, along with a portion of the sliding phase, occur at the bow of the ship, which is the primary region for ice-breaking. When the ship comes into contact with the ice layer, the stem of the bow initially engages with the ice, exerting compressive and shear forces that lead to the fracturing of the ice. As the bow advances and the contact area increases, the crushing force gradually intensifies, resulting in the formation of circular or wedge-shaped cracks. With the ship's continued progression, the vertical component of the force acting on the ice induces bending failure.

The newly formed ice floes are accelerated and rotated by the ship's propulsion, encountering resistance from waves and hydrostatic pressure. Due to frictional forces, the floating ice first rotates and surfaces at the edge of the intact ice until it aligns parallel to the ship's surface. Upon completion of the rotation, the changing motion of the ice fragments generates an impact force on the ship. During this period, the top surface of the rotating ice is pressed against the ship by the water, creating significant normal and frictional forces. Subsequently, it is further pushed downward along the ship's surface by other newly formed ice floes. At higher ship speeds, the vessel induces the floating ice to rotate, and the water flow cannot promptly fill the gap between the ice and the ship, leading to a sharp increase in resistance, which is known as ventilation phenomenon. As the icebreaker advances, the broken ice floes rotate, submerge, and separate. Some ice floes are displaced beneath the intact ice layer, while others continue to slide downward along the hull.

,Non-smooth discrete element method also known as Contact Dynamics or Impulse-Based Dynamics, which employs implicit time integration and the complementarity method to manage multi-body contact (Servin et al., 2014). This allows Non-smooth discrete element method (NDEM) to use larger time step while maintaining computational stability and convergence. Lubbad and Løset (2011) developed a real-time numerical model using the PhysX engine to simulate ship-floating ice interactions. Their 2D model focuses on contact damage near the waterline, while the 3D model treats broken ice floes as rigid bodies interacting with the hull. Similarly, Metrikin (2014) created a software framework for simulating offshore vessels in floating ice, covering both intact and broken ice conditions. However, these models primarily focus on ice loads near the waterline and lack detailed collision force calculations. Yang et al. (2021) applied the Bullet engine to simulate ship-broken ice interactions, using the same collision duration estimation method to calculate ice resistance and analyze ship maneuverability in broken ice. This paper simulates icebreaker interacts with pre-sawn ice based on the NDEM method, analyzing ice clearing phenomena at different ice thicknesses and speeds, and comparing the results with empirical formulas.

NUMERICAL MODELS

SIMULATION SETTING

The simulation is conducted based on the full-scale United States Coast Guard (USCG) Heavy Polar Icebreaker (HPIB), with specific parameters referenced from Wang et al. (2018). The simulation scenario is set up as shown in Figure 1, where the hull moves at a constant speed within a channel formed by two fixed layers of ice, colliding with pre-sawn ice arranged ahead. At the far end, a fixed wall restricts the forward movement of the pre-sawn ice. The geometric parameters of the ice field are illustrated in Figure 2. The total length of the pre-sawn ice

ensures complete coverage of the ship's bottom, and the overall width of the channel, denoted as w, is 33.8 meters. Each piece of pre-sawn ice has an angle of 80 degrees, a length of 7.4 meters, and a width equal to one-fourth of the channel's width.

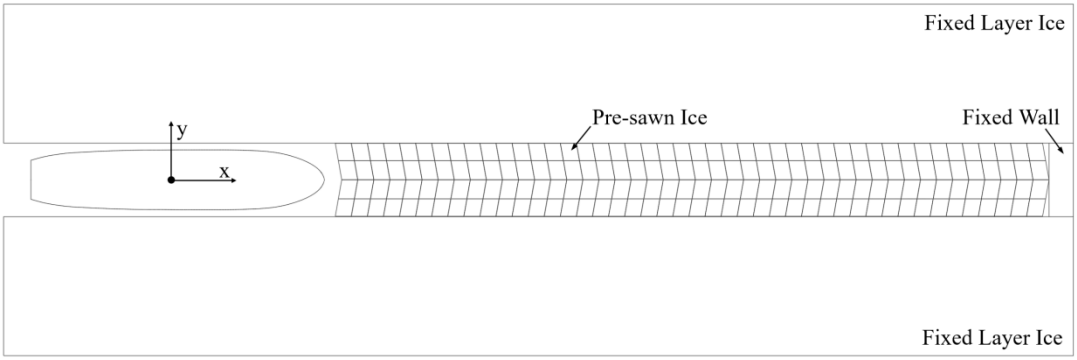

Figure 1 Simulation setup

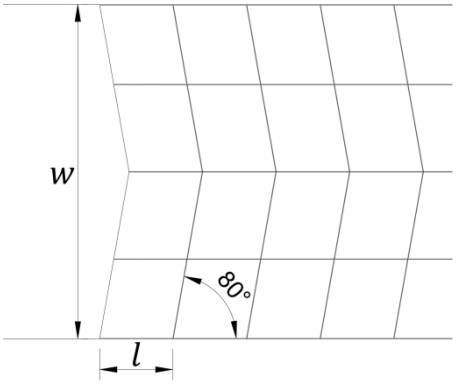

Figure 2 The geometric dimensions of the ice field

COLLISION DETECTION AND FORCE

Collision detection is a crucial technology for ensuring the authenticity and stability of ship-ice interactions. In this study, collision detection is conducted based on the Unity3D platform. The two-phase collision detection method is an efficient approach designed to reduce computational complexity and improve real-time performance. It consists of the broad-phase and narrow-phase stages, which progressively filter out unnecessary computations to ultimately determine actual collisions. The primary goal of the broad-phase is to quickly eliminate object pairs that are unlikely to collide, retaining only those that have the potential for intersection. In this study, Axis-Aligned Bounding Box (AABB) is used for broad-phase collision detection, representing objects with their minimum and maximum coordinate values. A simple interval overlap test is performed to determine whether two objects are likely to intersect. The narrow-phase stage performs further precise geometric calculations on the potential collision pairs identified in the broad-phase. It determines whether a collision has actually occurred and computes key information such as collision points and normal vectors. In this study, both ice floes and the ship are approximated using convex hulls to construct the actual collision bodies. The Gilbert-Johnson-Keerthi (GJK) algorithm, an efficient convex shape collision detection method, is employed. GJK determines the minimum distance between two objects using the Minkowski Difference. If the Minkowski Difference contains the origin, it indicates that a collision has occurred.

For a simple single-point collision, the collision impulse can be calculated based on elastic collision as

$$\lambda = \frac{-(1+e)(V_{rel} \cdot n)}{\frac{1}{m_1}+\frac{1}{m_2}} \tag{1}$$

where e is the coefficient of restitution, where $e = 1$ represents a perfectly elastic collision. V_{rel} is the relative velocity of the two objects at the collision point, and n is the collision normal vector. m_1 and m_2 are the masses of the two objects. When a ship squeezes ice, local crushing damage always occurs in the ice. Therefore, e is set to a very small value, 0.01. For complex multi-point collisions between ship-ice and ice-ice, the problem is solved by iteratively solving the Mixed Linear Complementarity Problem (MLCP):

$$\begin{bmatrix} M & -J_n & J_t \\ J_n^T & 0 & 0 \\ J_t^T & 0 & 0 \end{bmatrix} \begin{bmatrix} \Delta u \\ \lambda_n \\ \lambda_t \end{bmatrix} + \begin{bmatrix} 0 \\ \gamma_n \\ \gamma_t \end{bmatrix} = \begin{bmatrix} 0 \\ \alpha \\ \beta \end{bmatrix} \tag{2}$$

Where M is the mass matrix of the objects, and J is the contact constraint matrix, which includes information such as the collision normal. Δu represents the change in velocity of the objects. λ_n and λ_t are the unknown impulse in both the normal and tangential directions at the contact points. γ_n and γ_t are vectors containing the information of relative velocity and external impulse at the contact points. α and β are residual without physical meanings.

BUOYANCY

The buoyant force F_b and the resulting torque T_b acting on the ice floe are (see Figure 3)

$$\begin{cases} F_b = \rho_w V g \vec{n} \\ T_b = r_b \times F_b \end{cases} \tag{3}$$

where ρ_w is the water density, V is the submerged volume, and $\vec{n}$ is the unit vector in the vertical upward direction. The buoyant torque is obtained by taking the cross product of the buoyant force F_b and r_b, where r_b is the vector from the center of mass of the ice floe to the center of buoyancy. The submerged volume is calculated by accessing and processing the mesh data of the ice. The mesh of the ice floe is composed of multiple triangles. Each triangle and the origin $o(0,0,0)$ can form a tetrahedron. The volume of the ice floe can be calculated by summing the signed volumes of each tetrahedron (Dickheiser, 2006).

$$V = \frac{1}{6}\sum_{i=0}^{n}(a_i \times b_i) \cdot c_i \tag{4}$$

where a_i, b_i, and c_i are the vectors of the three vertices of the i-th triangle with the origin $o(0,0,0)$ respectively.

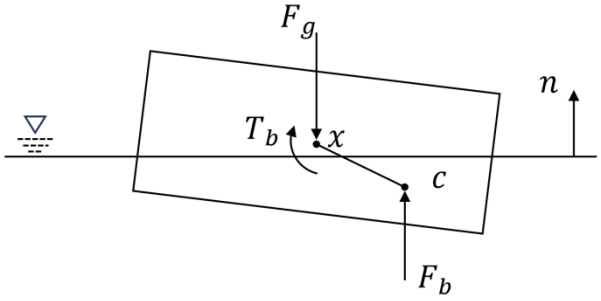

Figure 3 Buoyancy force and torque acting on the ice floe

FLUID FORCE

The method proposed by Soliman et al. (2024) is introduced to calculate the 6-DoF fluid forces on the ice floes. Under moderate Reynolds number conditions, the magnitudes of lift and drag forces acting on a flat plate in steady flow are

$$|F_l| = \frac{1}{2} C_l \rho_f A |u|^2 \tag{5}$$

$$|F_d| = \frac{1}{2} C_d \rho_f A |u|^2 \tag{6}$$

where ρ_f is the fluid density, A is the area of the flat plate, u is the flow velocity, and C_l and C_d are the lift and drag coefficients, respectively.

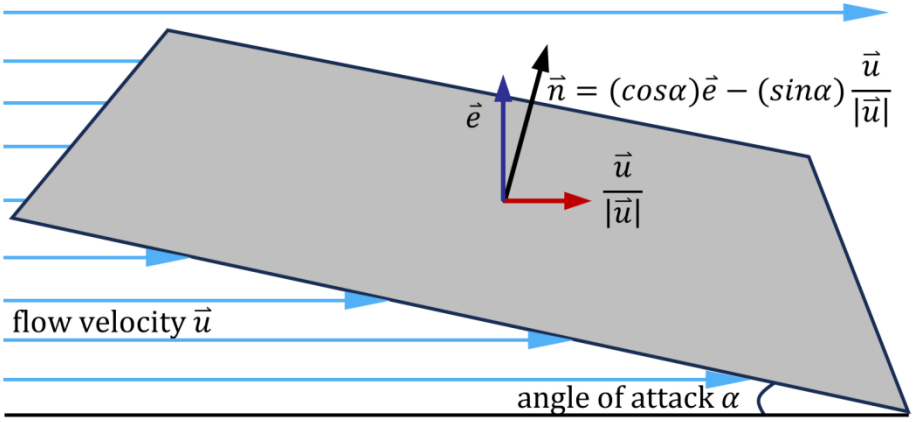

Figure 4 Demonstrate a flat plate in flow.

The angle of attack determines the lift and drag coefficients. Based on the experimentally measured data for lift and drag coefficients, the following formula can be used for approximate fitting (Caplan and Gardner, 2007)

$$\begin{cases} C_l = sin2\alpha \\ C_d = 2\sin^2\alpha \end{cases} \tag{7}$$

The direction of drag is opposite to the fluid velocity direction $\frac{\vec{u}}{|\vec{u}|}$, while the direction of lift is orthogonal to $\frac{\vec{u}}{|\vec{u}|}$. Therefore, the resultant force acting on the plate is

$$F = |F_l|\vec{e} - |F_d|\frac{\vec{u}}{|\vec{u}|} = -\rho_f A|\vec{u}|\langle\vec{u},\vec{n}\rangle\vec{n} \tag{8}$$

This results in a parameter-free expression for lift and drag on a flat plate in steady flow. The ice floe is composed of multiple triangular facets. The sum of the resultant forces on each triangular facet represents the total lift and drag forces acting on the ice floe, which is

$$F = -\frac{1}{2}\int \rho_f |\vec{u}|\langle\vec{u},\vec{n}\rangle\vec{n}dA \tag{9}$$

The fluid lift, drag, and buoyancy forces are combined into γ_n and γ_t to solve the MLCP problem in order to obtain the trajectory of the ice floe.

RESULTS

The simulation of the ship displacing pre-cut ice is shown in Figure 5. As the ship advances,

the ice floes first flip and then slide along the hull bottom. The two outer rows of ice floes, under the influence of the ship's hull, undergo flipping and subsequently slide within the side gaps of the hull. The two middle rows of ice floes are effectively pushed aside by the ship, with some being displaced outside the navigation channel and no longer in contact with the hull. The simulation reproduces the effective ice-clearing phenomenon of this heavy icebreaker, preventing ice floes from sliding along the hull bottom for an extended period and thereby avoiding additional frictional resistance.

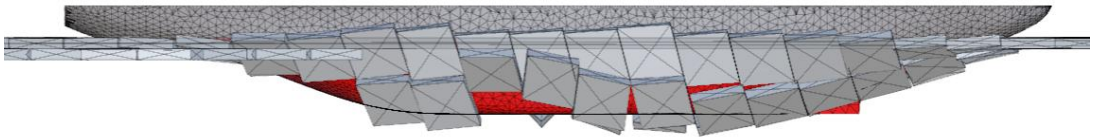

(a) Side view, $h = 1.5\text{m},\ \text{v} = 2\text{m/s}$

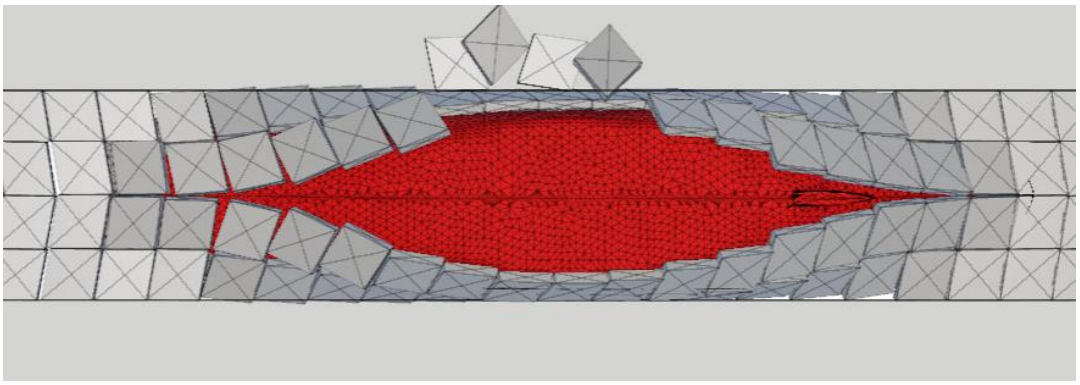

(b) Bottom view $h = 1.5\text{m},\ \text{v} = 1\text{m/s}$

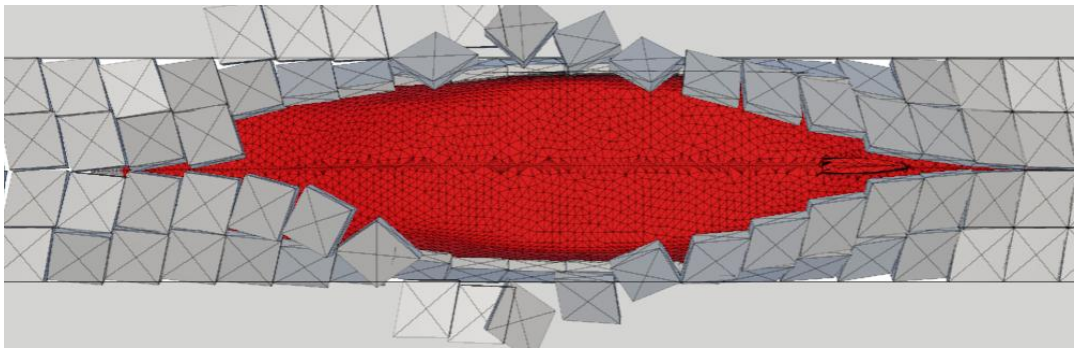

(c) Bottom view $h = 1.5\text{m},\ \text{v} = 1.5\text{m/s}$

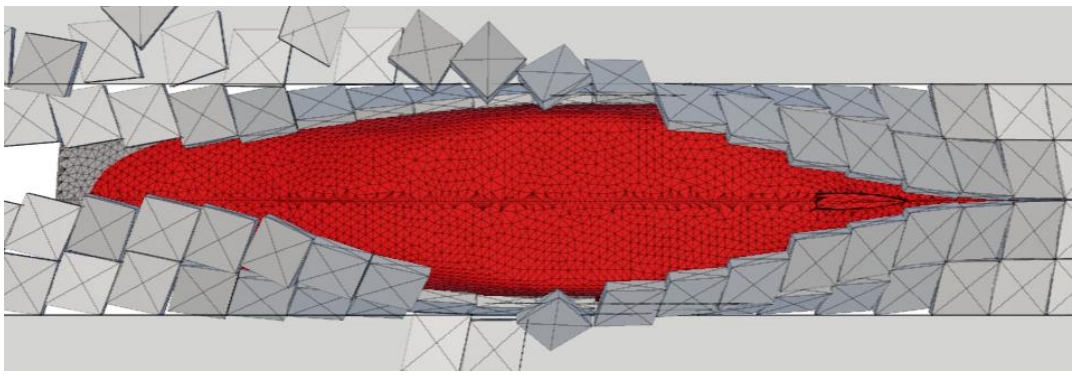

(d) Bottom view $h = 1.5\text{m},\ \text{v} = 2.0\text{m/s}$

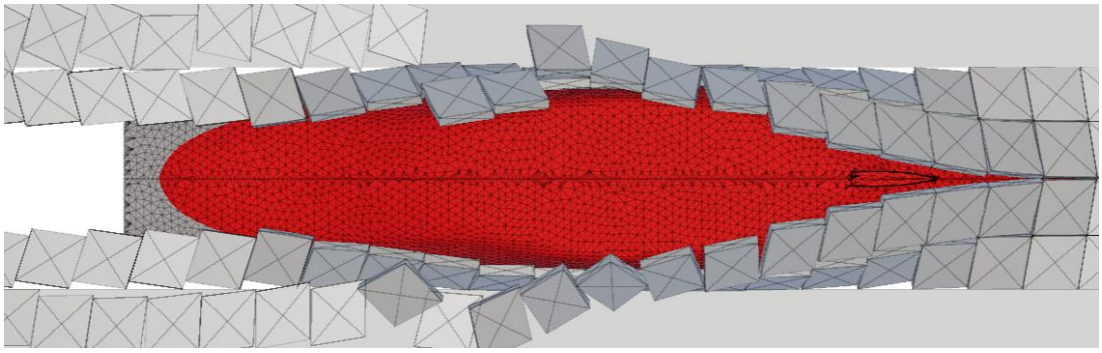

(e) Bottom view $h = 1.5\text{m},\ \text{v} = 2.5\text{m/s}$

Figure 5. Simulation of ice-clearing process

From subfigures (b), (c), (d), and (e) in Figure 5, it can be observed that at low speeds, ice floes displaced by the hull tend to remerge at the stern and come into contact with the hull again. As the ship speed increases, the two middle rows of ice floes are pushed far enough away by the hull, making it difficult for them to resurface and recontact the hull within a short time. At the maximum speed of 2.5 m/s, the same phenomenon occurs for the ice floes on both sides. In summary, at lower speeds, ice floes are more likely to accumulate near the bow, sliding closely along the hull and remerging at the stern. At higher speeds, the ship transfers greater kinetic energy when colliding with the ice, pushing the ice conditions further to the sides and preventing remerging at the stern.

The ice-clearing force consists of two components: the ship-ice collision force, which is the normal force F^n, and the resulting frictional force, which is the tangential force F^t. The submerged resistance is taken as the average of the x-direction components of these two forces, F_x^n and F_x^t. In the simulation, the x-direction ice collision force and tangential frictional force acting on the ship are shown in Figure 6. Initially, as the ship enters the ice field, the hull bottom is not yet fully covered by ice floes, and the collision force exhibits a trend of increasing in absolute value. Therefore, the submerged resistance is calculated as the average of the latter 50% of the time history of the collision force. It should be noted that the collision force exhibits a few individual points with extremely large peak values, which significantly deviate from the overall trend and are considered outliers. These outliers may be caused by abnormal excessive overlap between the ice floes and the ship's hull.

After subtracting the mean value from the collision force, a Fourier transform is performed on it, and the frequency spectrum is shown in Figure 7. It can be observed that, apart from the peak at zero frequency, the fundamental frequency appears at 0.27 Hz, and the frequencies corresponding to the remaining peaks are approximately integer multiples of the fundamental frequency. With an ice floe length of 7.4 meters and a ship speed of 2 meters per second, the ship-ice contact frequency is calculated to be 0.2703 Hz. This value coincides with the fundamental frequency extracted from the frequency spectrum. This indicates that the peaks in the ship-ice collision force predominantly occur when the ship initially comes into contact with a new row of ice floes.

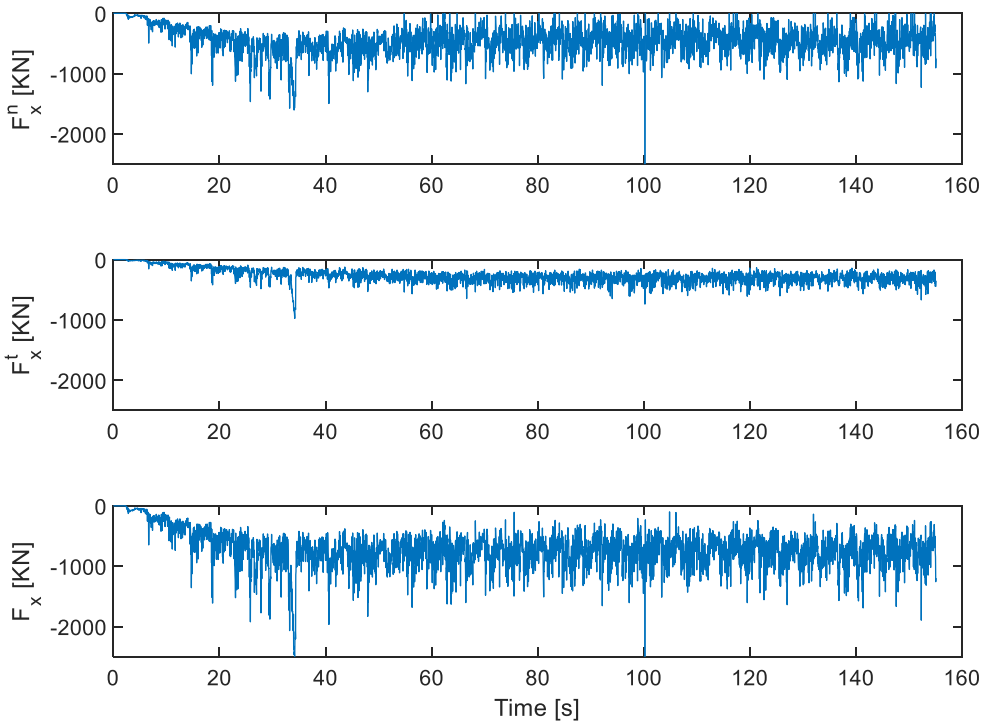

Figure 6. The time history of the ship-ice collision force. ($h_i = 1.5m,\ V = 2m/s$)

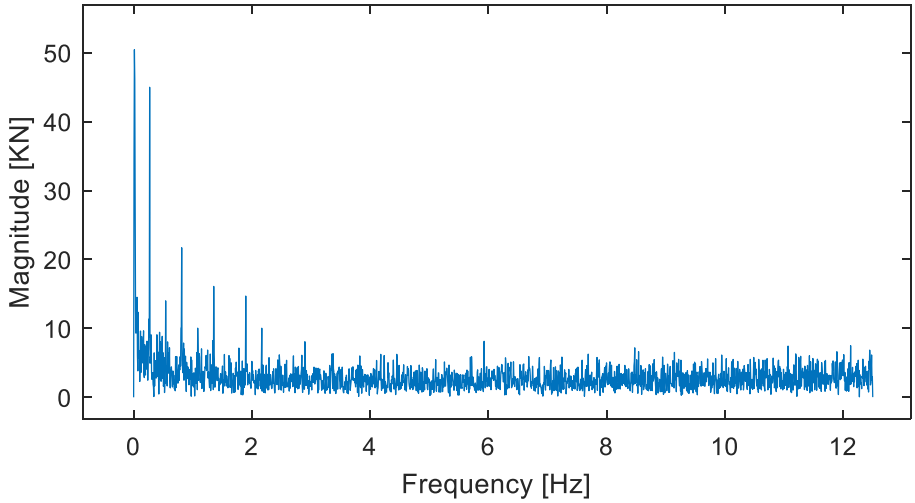

Figure 7. Performing Fourier transform on the ship-ice collision force. ($h_i = 1.5m,\ V = 2m/s$)

The heavy icebreaker possesses significantly greater propulsion power, enabling it to break through thicker ice layers and maintain higher navigation speeds. Therefore, this study conducted ice-clearing simulations under ice thicknesses of 1.5 meters and 2.5 meters, with ship speeds ranging from 1 to 2.5 meters per second. The ice-clearing resistance for each operating condition was obtained and is shown in Figure 8. It can be observed that as the ship speed increases, the ice-clearing resistance also increases. At an ice thickness of 2.5 meters, a turning point appears when the ship speed increases from 2 m/s to 2.5 m/s. Additionally, a comparison was made with the submerged resistance component in Lindqvist ice resistance formula. At 1.5m ice thickness, the simulated submerged ice resistance generally follows the

trend of the Lindqvist formula, with the gap increasing as speed increases. At 2.5m ice thickness, the simulated resistance is significantly different, being 20% higher than the Lindqvist estimate results.

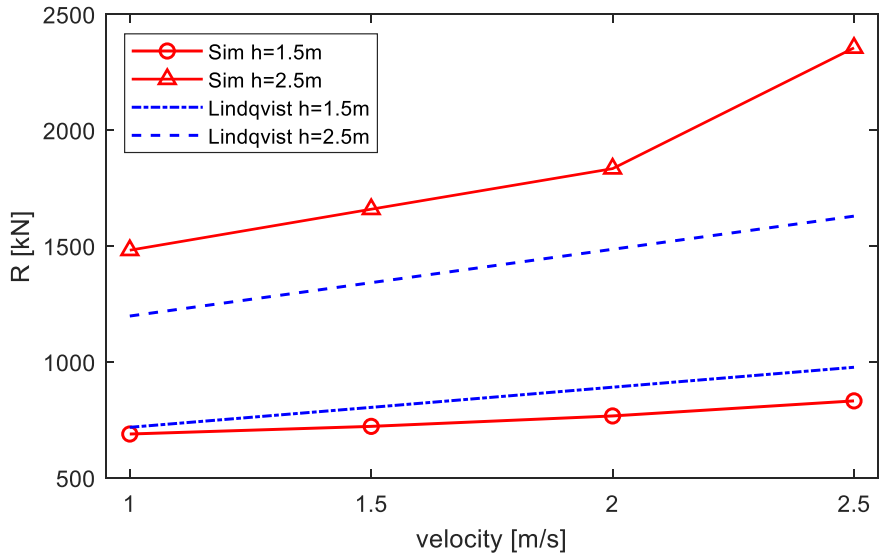

Figure 8. Ice-clearing resistance under different ice thicknesses and ship speeds.

CONCLUSIONS

This paper establishes a simulation model for ship towing pre-sawn ice based on the non-smooth discrete element method. Efficient collision detection and iterative solving of the MLCP problem are employed to calculate the collision impulses between ship-ice and ice-ice interactions. A param-free model for ice lift and drag forces is constructed based on the Morison equation and experimental data, while real-time buoyancy calculation is introduced to accurately account for the hydrostatic and hydrodynamic forces acting on the ice. Simulations of ice resistance under varying speeds and ice thicknesses were conducted using a heavy icebreaker, yielding the following conclusions:

1) The proposed model is capable of predicting the underwater trajectory of ice under ship-ice interaction.

2) The bottom of the ship is not entirely covered by ice. At low speeds, ice accumulates at the bow, slides along the ship's sides, and reunites at the stern. At higher speeds, the ice is pushed sufficiently far away by the hull, preventing further contact. This validates that the hull design of this heavy icebreaker effectively disperses broken ice, reducing contact and minimizing submerged resistance.

3) Compared with the Lindqvist estimate, submerged resistance shows a similar trend with small differences at low ice thickness. However, at high ice thickness and speed, the difference increases, exceeding the Lindqvist result by 20%.

It should be noted that the numerical method in this paper still requires more model test data for validation, and the applicability of the Lindqvist formula under thick ice conditions remains worth investigating.

ACKNOWLEDGEMENTS

This work is supported by National Key Research and Development Program (2022YFE0107000), Young Scientists Fund of National Natural Science Foundation of China (No. 52301331), Science and Technology Commission of Shanghai Municipality Project (23YF1419900, 22DZ1204403), General Projects of National Natural Science Foundation of China (52171259), and High-tech ship research project of Ministry of Industry and Information Technology ([2021]342).

REFERENCES

Caplan, N., Gardner, T., 2007. A mathematical model of the oar blade–water interaction in rowing. Journal of sports sciences 25 (9), 1025-1034.

Dickheiser, M., 2006. Game Programming Gems 6 (Book & CD-ROM)(Game Development Series). Charles River Media, Inc.

Lubbad, R., Løset, S., 2011. A numerical model for real-time simulation of ship–ice interaction. Cold Regions Science and Technology 65 (2), 111-127.

Metrikin, I., 2014. A software framework for simulating stationkeeping of a vessel in discontinuous ice.

Servin, M., Wang, D., Lacoursière, C., Bodin, K., 2014. Examining the smooth and nonsmooth discrete element approaches to granular matter. International Journal for Numerical Methods in Engineering 97 (12), 878-902.

Soliman, Y., Padilla, M., Gross, O., Knöppel, F., Pinkall, U., Schröder, P., 2024. Going with the Flow. ACM Transactions on Graphics (TOG) 43 (4), 1-12.

Valanto, P.U., 1989. Experimental and theoretical investigation of the icebreaking cycle in two dimensions. University of California, Berkeley.

Wang, J., Akinturk, A., Brown, J., Muselet, C., Millan, J., 2018. Model Tests of the United States Coast Guard Heavy Polar Icebreaker Indicative Designs, OTC Arctic Technology Conference. OTC, p. D023S013R004.

Yang, B., Sun, Z., Zhang, G., Wang, Q., Zong, Z., Li, Z., 2021. Numerical estimation of ship resistance in broken ice and investigation on the effect of floe geometry. Marine Structures 75, 102867.